Available online at www.sciencedirect.com

ScienceDirect

Acta Materialia 61 (2013) 7189–7196

Acta MATERIALIA

www.elsevier.com/locate/actamat

Anomalous yielding in the complex metallic alloy $Al_{13}Co_4$

C. Walter [a], J.M. Wheeler [b], J.S. Barnard [a], R. Raghavan [b], S. Korte-Kerzel [c,1], P. Gille [d], J. Michler [b], W.J. Clegg [a,*]

[a] Department of Materials Science and Metallurgy, University of Cambridge, 27 Charles Babbage Rd, Cambridge CB3 0FS, UK

[b] Laboratory for Mechanics of Materials and Nanostructures, EMPA, Swiss Federal Laboratories for Materials Testing and Research, Feuerwerkerstr. 39, CH-3602 Thun, Switzerland

[c] Friedrich-Alexander-University Erlangen-Nuremberg, Martensstrasse 5, 91058 Erlangen, Germany

[d] Ludwig-Maximilians-Universität München, Theresienstrasse 41, 80333 München, Germany

Received 16 July 2013; received in revised form 5 August 2013; accepted 10 August 2013
Available online 13 September 2013

Abstract

The single crystal deformation behaviour of orthorhombic $Al_{13}Co_4$ has been studied below the brittle-ductile transition temperature observed in bulk material from room temperature to 600 °C, using indentation, microcompression and transmission electron microscopy. At room temperature, slip occurred most easily by dislocation motion on the (0 0 1)[0 1 0] slip system, as observed in the ductile regime at high temperatures. However, as the temperature was increased towards 600 °C, the slip pattern changed to one consisting of linear defects running perpendicular to the loading axis. Serrated flow was observed at all temperatures, although at 600 °C the magnitude of the serrations decreased. Anomalous yielding behaviour was also observed above 226 °C, where both the yield and the 2% flow stress increased with temperature, almost doubling between 226 and 600 °C. It has been suggested that this might arise due to the increasing stability of orthorhombic $Al_{13}Co_4$ with respect to the monoclinic form with increasing temperature. This is shown to be consistent with the theoretical predictions that exist.

Keywords: Intermetallics; Al alloys; Plastic deformation; Dislocation

1. Introduction

Materials with large unit cells, such as complex metallic alloys, might be expected to contain dislocations with correspondingly large Burgers vectors. As both the line energy of the dislocation and the resistance of the crystal lattice to dislocation motion scale with the square of the Burgers vector, such materials should be exceptionally strong. However, above a critical temperature, T_{BDTT}, typically between 0.6 and 0.8 T_M [1,2], these materials deform at quite low stresses to high strains, often without showing work hardening [1].

Above T_{BDTT}, it has been shown that dislocations of varying complexity form. This may involve dissociation by climb [3] or by glide [4], and may be accompanied by some phase transformation in the material around the dislocation core that reduces the magnitude of the Burgers vector [5]. When orthorhombic (o) $Al_{13}Co_4$ is deformed above the brittle–ductile transition temperature of approximately 600 °C the reduction in Burgers vector is achieved by the formation of a partial dislocation, which must leave a trailing fault behind it [4]. In this case, the fault is a slab of the monoclinic (m) phase a few nanometres in thickness. However, deformation at temperatures below T_{BDTT} has not been studied due to catastrophic failure dominating the behaviour.

The aim of this paper, therefore, is to investigate whether such materials might deform plastically at temperatures below T_{BDTT} and, if so, how this might occur. Low temperature deformation has been studied both by nanoindentation and micropillar compression. The latter allows

* Corresponding author. Tel.: +44 1223 334470.
E-mail address: wjc1000@cam.ac.uk (W.J. Clegg).
[1] Present address: Institute of Metallurgy and Metal Physics, RWTH Aachen University, Kopernikusstr. 14, 52074 Aachen, Germany.

1359-6454/$36.00 © 2013 Acta Materialia Inc. Published by Elsevier Ltd. Open access under CC BY license.
http://dx.doi.org/10.1016/j.actamat.2013.08.023

individual slip systems to be investigated by uniaxially compressing an appropriately oriented single crystal, while the small size helps suppress cracking [6,7].

2. Experimental

Experiments were carried out on an $Al_{13}Co_4$ single crystal with an orthorhombic crystal structure, made by the Czochralski method [8]. A preliminary study of the flow behaviour was carried out using nanoindentation (Nanoindenter XP, MTS). More detailed studies of the flow behaviour were then made using microcompression. Except where otherwise stated, the work was carried out on micropillars with a diameter of 2 μm and an average height of 7.5 μm. Effects of size were also investigated using micropillars with diameters ranging from 0.7 to 4 μm. All pillars were made using focused ion beam milling (Helios Nanolab, FEI). The final beam current used was 48 pA, producing pillars with a taper of approximately 2°. During the milling process, the built-in image recognition software (RunScript) was used to decrease the drift of the ion beam during milling. This enabled the fully automated production of the micropillars, minimizing any possible difference in their geometries. Much of the work was carried out on pillars where the crystal was oriented to give a Schmid factor of 0.5 on the (0 0 1)[0 1 0] slip system, so that the axis of the pillar was [0, 1.174, 1]. To investigate the possibility of slip on other systems, tests were also carried out on pillars where the axes of the pillars were parallel to the [1 0 0], [0 1 0] and [0 0 1] crystal directions, where the Schmid factor was zero on the (0 0 1)[0 1 0] slip system.

Microcompression was carried out using an in situ nanoindenter [9] (Alemnis, CH), with a 5 μm diameter diamond punch, under displacement control at a rate of 5 nm s^{-1}. This produced a strain rate of approximately 7×10^{-4} s^{-1}. The indenter had been modified by incorporating a water-cooled frame and independent tip and sample heating, yielding typical thermal drift values of less than 0.02 nm s^{-1} due to the thermally stable system frame and precise temperature matching of the sample and indenter temperatures [10,11]. This enabled testing at temperatures up to 600 °C. Above this temperature, it was difficult to image the heated sample due to thermionic emission saturating the secondary electron detector [9]. Testing was first carried out at low temperature, and flow was generally characterized using the flow stress at a plastic strain of 0.02. However, the yield stress, where the stress-strain curve first deviated from linearity, was also measured. The temperature was then raised and allowed to stabilize, with four or five samples being compressed at each temperature. After carrying out tests at the maximum temperature, the samples were cooled and a further set of tests was carried out at room temperature. In all cases the results obtained at room temperature both before and after heating were consistent with one another, showing that there were no changes due to the heating cycle.

Slip patterns in the deformed pillars were studied by preparing thin lamellae, approximately 100 nm thick, by ion milling (Helios Nanolab, FEI). Microstructural analysis was carried out by transmission electron microscopy (TEM) using a Philips CM30 transmission electron microscope operated at 300 kV.

3. Results and discussion

The average values of hardness and Young modulus were 10 and 200 GPa, respectively, with less than 10% difference in the values for the different crystal faces (Table 1). As might be expected for a material with a high ratio of the hardness to the Young modulus, there was no significant pile-up around the indentation. Parallel ledges on two of the three faces of the residual imprint could be observed in the scanning electron microscope (SEM; Fig. 1), where the sample surface is parallel to (0 1 0). The (0 0 1)[0 1 0] slip system, observed in high temperature compression, would therefore run perpendicular to the surface. However, the traces of the slip planes do not appear to be aligned with the (0 0 1) plane, suggesting that slip can occur on other systems. There was also some cracking, although the cracks formed near the edges of the pyramidal imprint, rather than at the corners.

Tests carried out at indentation strain rates, $\dot{\varepsilon}_I$, defined as $\dot{\varepsilon}_I = \dot{h}/h \approx \dot{P}/2P$, where h is the displacement and P is the load, from 0.01 to 0.4 s^{-1} showed that deformation appeared to be homogeneous, although very small pop-ins could be seen (Fig. 2). The change in the hardness with strain rate was measured (Fig. 3) using constant strain rate tests as opposed to stress jump tests, and setting the flow stress, σ, as one-third of the hardness, the strain rate sensitivity, m, during nanoindentation was estimated as 0.06 GPa, using

$$m = \frac{d\sigma}{d(\ln \dot{\varepsilon})} \quad (1)$$

Similar behaviour was observed in micropillar compression at room temperature (Fig. 4), where the value of m, using the 2% flow stress, was measured to be 0.08. The strain rate sensitivity can also be used to estimate the activation volume, using the expression

$$V = \frac{kT}{Sm} \quad (2)$$

where k is the Boltzmann constant, T is the temperature and S is the Schmid factor. Setting T to 298 K, S to 0.5 and m to either 0.08 for microcompression or 0.06 for

Table 1
The hardness, H, and Young modulus, E, measured by nanoindentation for crystals with axes parallel to [1 0 0], [0 1 0] and [0 0 1].

Orientation	[1 0 0]	[0 1 0]	[0 0 1]
H (GPa)	10.6 ± 0.4	10.2 ± 0.3	10.7 ± 0.5
E (GPa)	186 ± 14	213 ± 9	199 ± 15

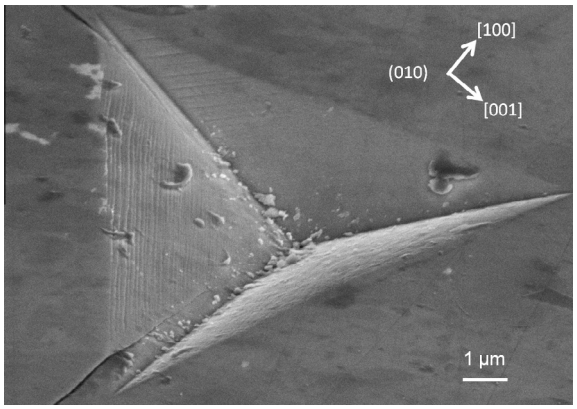

Fig. 1. Scanning electron micrograph of the residual imprint after nanoindentation with a Berkovich tip. Two of the three faces of the pyramidal imprint show a number of parallel ledges. These ledges are not aligned with the (0 0 1)[0 1 0] slip system observed in bulk and pillar compression.

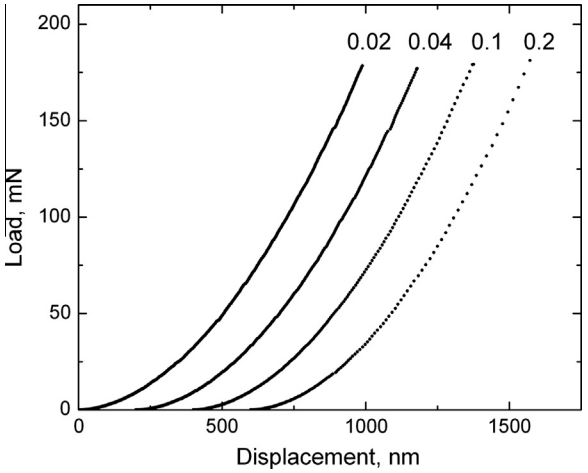

Fig. 2. Load–displacement curves from nanoindentation at different strain rates. Single measurement points are shown to confirm that the sampling rate was adequate to pick up serrations. The curves are shifted with respect to each other along the x axis for visibility.

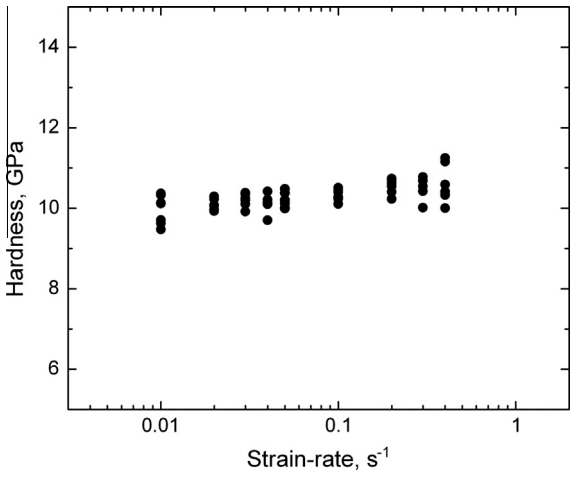

Fig. 3. The hardness measured by nanoindentation experiments at different strain rates.

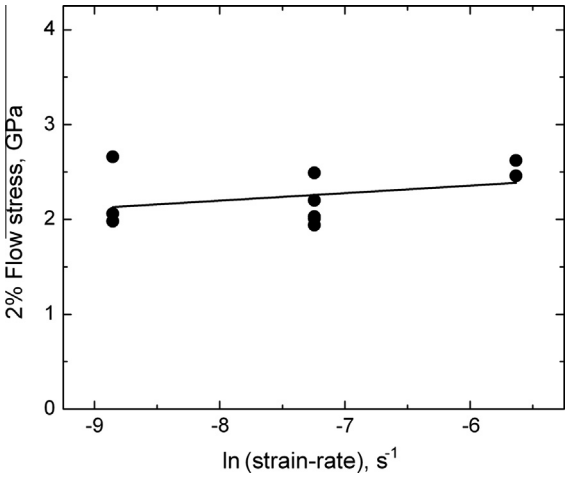

Fig. 4. The variation of 2% flow stress with strain rate for microcompressed pillars oriented so that the (0 0 1)[0 1 0] slip system is aligned at 45° to the pillar axis with a Schmid factor of 0.5.

indentation gives values of V equal to 0.1 and 0.06 nm^3, respectively. These can be compared with the data of Heggen et al. [1], who used the above expression to measure the activation volume and showed that it varied approximately inversely with the applied stress. Taking average values of 2 GPa for microcompression and 3.4 GPa for indentation, the tensile flow stresses in each case, Heggen's data gives $V = 0.12$ nm^3 at 2 GPa and $V = 0.07$ nm^3 at 3.4 GPa. The agreement between the two sets of values suggests that the underlying deformation mechanism is similar at both high and low temperatures.

Micropillar compression was also used to investigate the operative slip systems over a range of temperatures below T_{BDTT}. Generally, the reproducibility of the elastic and plastic behaviour was very good (Fig. 5), the flow stresses measured at any given temperature varying by no more than ±17%. The SEM showed clearly visible slip bands on all of the pillars (Fig. 6), except for one of those tested at 600 °C. The angle of the slip bands with respect to the loading axis and the direction of slip was consistent with the (0 0 1)[0 1 0] slip system that has been observed above T_{BDTT} [9]. This was the same for all pillars over the entire temperature range. The size and general appearance of the slip bands in the SEM appeared to be independent of the temperature of deformation (Fig. 6).

One might expect the predominant obstacle to flow in such materials to be dominated by the lattice resistance, so that the flow stress would be both rate and temperature dependent, decreasing approximately linearly with temperature. However, as can be seen from Fig. 7, both the yield stress and the 2% flow stress increased with temperature.

The values of the yield stress obtained by microcompression (Fig. 7) were greater than those obtained from measurements above T_{BDTT} on larger samples [1]. The most likely explanation, if the lattice resistance or a relatively weak obstacle dominates flow [12], is that this is associated with a difference in the strain rates between the bulk tests,

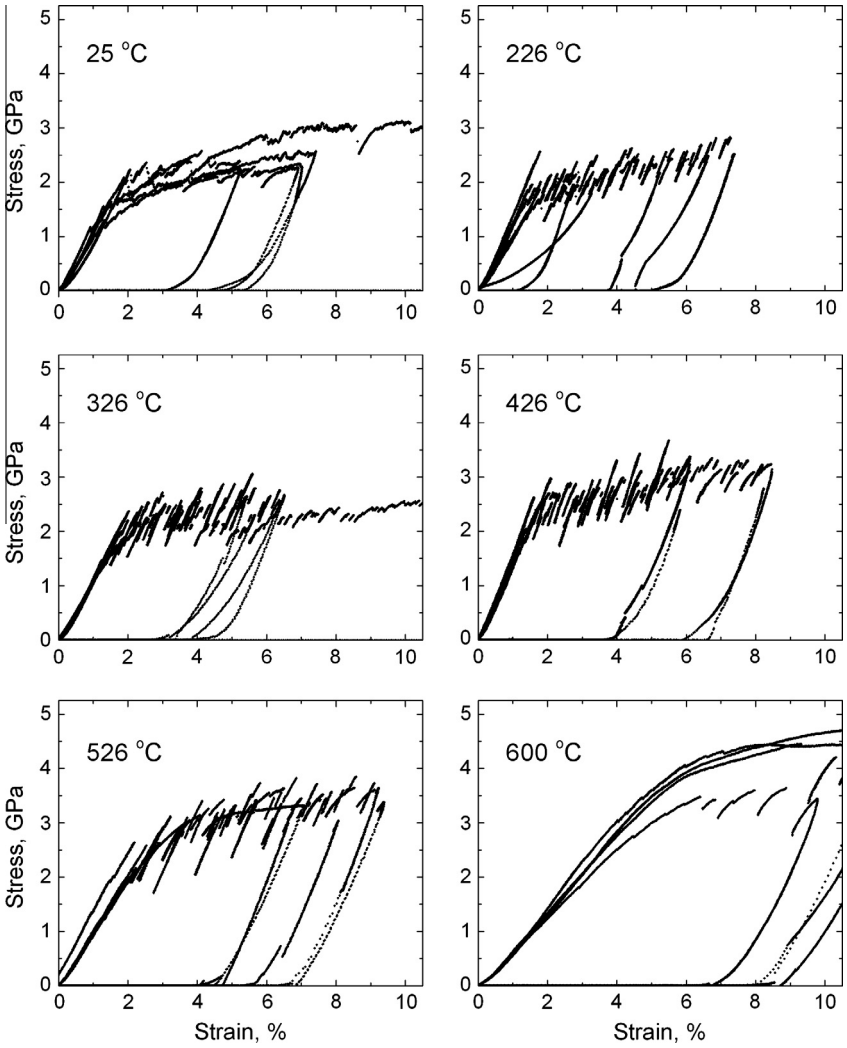

Fig. 5. Engineering stress–strain curves evaluated from the compression experiments at different temperatures.

carried out at $10^{-5}\,s^{-1}$, and the micropillar tests, carried out at $7 \times 10^{-4}\,s^{-1}$. Another possibility is that this difference is associated with size effects. To investigate this, a series of $Al_{13}Co_4$ pillars with radii ranging from 0.7 to 4 μm were compressed at a temperature of 226 °C. The aspect ratio of these pillars was between 2 and 4.5 and the displacement rate was adjusted to ensure that the strain rate was constant for the different pillar sizes. No significant change in flow stress was observed over this range of pillar sizes (Fig. 8). This suggests that any size effect, at least over this range, is small and that the yield and flow stresses measured in the bulk samples are genuinely lower than those measured in microcompression. This would also be consistent with the observation that the size effect in strong materials [13] is smaller than that commonly observed in face-centred cubic metals [14].

The stress–strain curves showed serrated flow (Fig. 5), with a maximum stress drop of approximately 0.5 GPa per serration being reached at 426 °C. At 600 °C, the serrations were greatly diminished. This serrated flow is in contrast to indentation where the load–displacement curves at room temperature were relatively smooth, possibly due to the greater constraint on flow in indentation. The magnitude of the serrations was also strongly influenced by the crystal orientation of the pillars (Fig. 9), suggesting that flow is associated with the crystallography of the material and that $Al_{13}Co_4$ does not behave in the same manner as a metallic glass, as has been suggested for $Mg_{17}Al_{12}$ [15]. Pillars with [1 0 0] orientation showed a great scatter in the onset of flow, varying from about 1.5 GPa to just over 5 GPa. Those samples where deformation began at the higher stresses also showed extremely large yield drops, most likely due to cracking. However, for the pillars with [0 1 0] and [0 0 1] orientations, slip on different slip systems was observed at flow stresses of approximately 4 GPa. By measuring the angle of the slip plane trace to the pillar axis and the direction in which slip occurred, the Schmid factors were estimated to be 0.47 and 0.45 for the [0 1 0] and [0 0 1] orientations, respectively. In both cases, the compressive flow stresses at room temperature were greater than 4 GPa (Fig. 9), compared with flow stresses of approximately 2 GPa in the pillars where the (0 0 1)[0 1 0] system

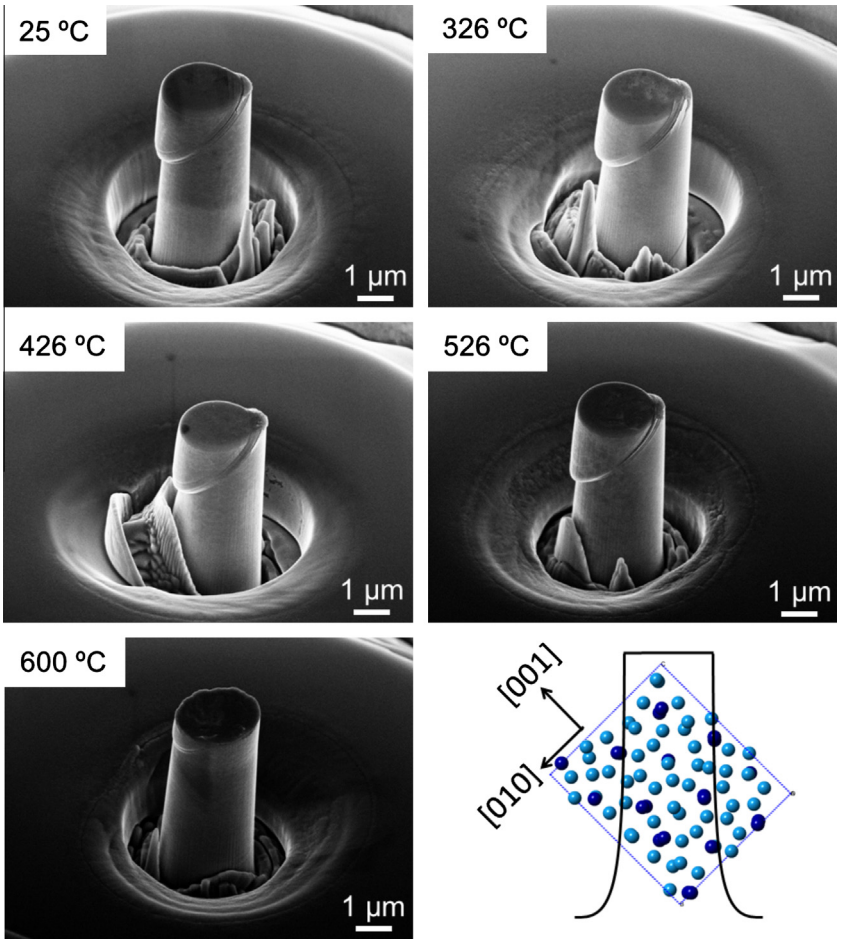

Fig. 6. Micropillars after compression at 25, 326 and 526 °C, with slip bands clearly visible on the surfaces. The sketch shows how the unit cell is oriented with respect to the pillars with the (001)[010] slip system aligned at 45° to the pillar axis having a Schmid factor of 0.5.

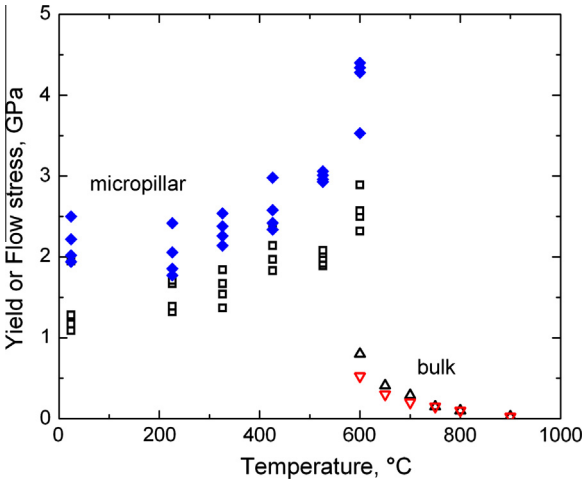

Fig. 7. Yield and 2% flow stress of the micropillars at different temperatures. The points labelled bulk are the upper and lower yield points from larger scale compression experiments [1].

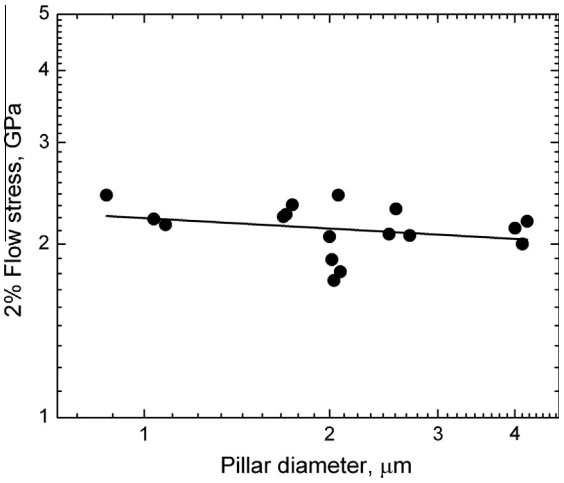

Fig. 8. Flow stress of micropillars with different diameters compressed at a constant temperature of 226 °C. The aspect ratio and strain rate were kept approximately constant.

was aligned for slip (Fig. 7). This is consistent with the weakest slip system being (001)[010] [1] and also with the measured hardness being more than three times the flow stress on the (001)[010] slip system, as flow would be required on these other, harder slip systems, to accommodate the indentation [16].

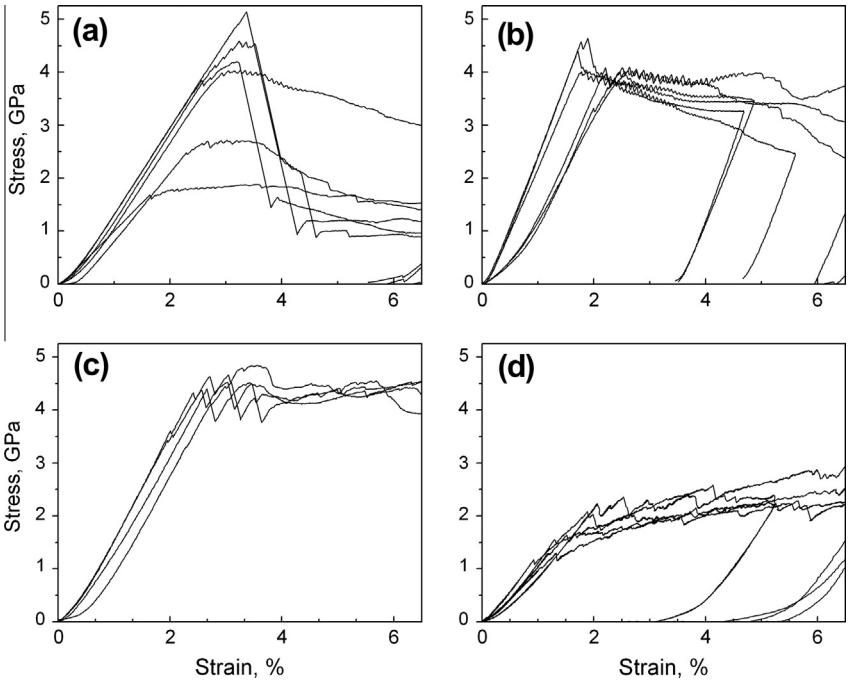

Fig. 9. Engineering stress–strain curves at room temperature for micropillars with different orientations: (a) [100], (b) [010], (c) [001] along the compression axis and (d) with the (001)[010] system aligned for slip as used for the temperature series.

For samples oriented for slip on the soft slip system, slip bands propagated completely through the pillar with the materials being displaced along the same plane for a substantial distance (Fig. 10a). This figure also shows the slip patterns observed in micropillars compressed at room temperature, at 426 °C (Fig. 10b) and at 600 °C (Fig. 10c). At room temperature, deformation occurred by the movement of dislocations, marked D, on the (001)[010] slip system, marked S, although some dislocation motion was observed off the (001) plane.

Deformation off the (001) plane was more apparent in micropillars deformed at 426 °C rather than at room temperature, with a greater number of dislocations (Fig. 10b). Additionally at 426 °C, linear defects, marked L, lying in a plane perpendicular to the pillar axis, were observed. These were predominantly seen in the portion above the slip plane and appeared to either start or end there, although they also formed at the pillar surface. These linear defects were not perfectly straight, but wandered slightly along the pillar axis, in a slightly wavy manner. They were closely spaced with separations from several to a few tens of nanometres, and all seemed to emerge from either a free surface, such as the side of the pillar, or from the (001) slip planes. The linear defects must, therefore, form after the onset of slip, suggesting that it is the presence of the free surface or the slip plane that enables the formation of the linear defects.

The deformation behaviour at 600 °C was more complex. Of the four samples tested, three showed slip lines of the type seen at lower temperatures, although the serrations in the stress–strain curves were substantially smaller in all but one micropillar. Unfortunately three of the membranes for TEM were destroyed during focused ion beam

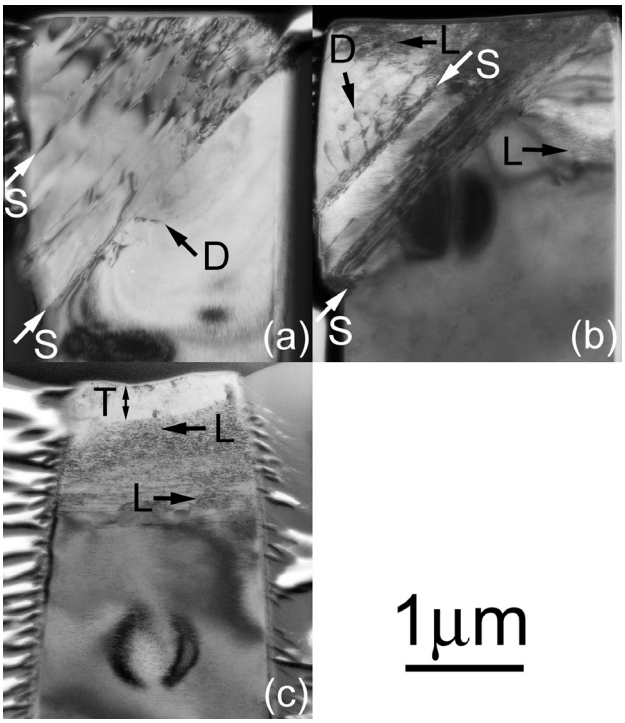

Fig. 10. Bright-field TEM images of the pillars deformed at (a) 25 °C (b), 426 °C and (c) 600 °C to show several defect types: slip planes (S) and dislocations (D) occur at low-to-mid temperatures (a) and (b); linear defects (L) occur at mid- to high temperatures (b) and (c). The 600 °C sample shows a 200 nm thick layer (T) at the top with a large tilt and twist. The apparent taper of the 600 °C sample is due to the preparation of the TEM lamella not going straight through the centre plane as the pillar was slightly bent.

milling and only one was available for examination. The stress–strain data showed small serrations, while the slip band tended to occur at one side of the pillar. In the sample examined by TEM, only linear defects could be seen, possibly because the slip plane was on one side of the sample.

The linear defects have finite (and variable) thickness and have a crystallography that is at variance with the bulk and a full quantitative analysis of these features in underway. As they are moving on a plane perpendicular to the free surface, the resolved shear stress acting on them would be zero, if they were conventional glide dislocations. This situation is not changed by the presence of the trailing fault, as the phase transformation does not give a reduction in the thickness of the material that makes up the fault. One concern was that this might be associated with a slight bending in the pillar deformed at 600 °C, but no such bending was observed in the pillar deformed at 426 °C, suggesting that the formation of these defects might be due to friction between the punch and the top surface of the pillar. However, the defects were observed to grow at substantial distances away from the top surface. All of these linear defects were observed to grow from free surfaces or from slip planes, suggesting that the prevalence of these defects, compared with that in a bulk sample, is associated with the greatly increased surface area:volume ratio in the micropillar. However, as they form after the initial slip has occurred, there would be no effect on the measured yield stress. Their effect must therefore be limited to work hardening. However, at least below 600 °C, the rate of increase in the yield stress and 2% flow stress with temperature are very similar (Fig. 7), suggesting that the increase in flow stress is not associated with the formation of lateral defects. At 600 °C, the increase in the flow stress was slightly greater than expected, and this may be associated with a contribution from the movement of lateral defects.

The only feature specific to the 600 °C deformed pillar that was examined by TEM was a 200 nm thick layer at the top, marked T (Fig. 10c). This gave a selected area diffraction pattern similar to the main pillar material but with a large tilt and twist. However, the presence of a reflection corresponding to 0.205 nm (not shown) was also established in the top layer. This is consistent with the Al (2 0 0) reflection, suggesting that there has been some decomposition of the $Al_{13}Co_4$. This was unexpected, as the phase diagram shows that this phase exists up to at least 974 °C [17] but may be caused by reaction between the diamond punch and the Co, which has a range of carbides, present in $Al_{13}Co_4$. Unfortunately, as the other pillars were destroyed during milling, it was not possible to see whether this layer formed consistently at high temperature.

Anomalous yielding is usually attributed to either cross-slip of partial dislocations, as in Ni_3Al, or pinning of dislocations by solute atoms or vacancies, as in β-brass [18], and is often accompanied by serrated flow. Yield anomalies have been classified into two general types: velocity type and exhaustion type [19]. Exhaustion-type anomalies are ascribed to an anomalous evolution of the density of mobile dislocations and are usually characterized by zero steady-state strain rate sensitivity in combination with work hardening. Velocity-type anomalies are ascribed to anomalous evolution of the velocities of single dislocations and are usually characterized by positive strain rate sensitivity and much lower work hardening than exhaustion-type anomalies.

However, an alternative mechanism is also possible here. Heggen et al. [4] have shown that, in o-$Al_{13}Co_4$ above T_{BDTT}, dislocation motion on the (0 0 1)[0 1 0] slip system occurs by the motion of partial dislocations that leave, in their wake, a trailing fault of monoclinic m-$Al_{13}Co_4$ a few nanometres in thickness, and the measurements of the activation volume here suggest that a similar mechanism is operating at low temperatures. The formation of a partial dislocation enables a reduction of the Burgers vector, and hence misfit energy and the changes in misfit energy that arise as it moves. However, the formation of the fault requires extra energy for the orthorhombic to monoclinic phase transformation that would increase the resistance to dislocation motion.

The energy required for this phase transformation depends on the relative phase stabilities of these two phases. Taking the Al–Co phase diagram, the orthorhombic and monoclinic phases are both denoted as $Al_{13}Co_4$ in terms of their stoichiometry, with the orthorhombic phase on the Al-rich side of the monoclinic phase, and they coexist over a large temperature range [17], suggesting that their free energies are fairly similar. However, there are some indications as to how these might change with temperature. The relative phase stabilities have been calculated at 0 K [20,21] and both sets of calculations predict that both phases are theoretically unstable at 0 K. However, both phases are stabilized by the introduction of vacancies with increasing temperature, with the monoclinic phase eventually becoming theoretically stable at approximately 750 K [20]. These calculations also showed that the vacancies have a stronger stabilizing effect on the orthorhombic phase than on the monoclinic phase at 0 K. Thus, with the abundance of vacancies increasing with temperature, the relative phase stability of the orthorhombic phase compared to the monoclinic phase would be expected to increase with increasing temperature, increasing the energy change as o → m, and making dislocation motion more difficult with increasing temperature, as is observed.

4. Conclusions

The deformation behaviour of o-$Al_{13}Co_4$ has been studied from room temperature to 600 °C, the approximate brittle to ductile transition temperature. It has been shown that slip occurred most easily by dislocation motion on the (0 0 1)[0 1 0] slip system, as observed at higher temperatures, and measurements of the activation volume at room temperature were consistent with measurements at higher temperature, suggesting that the mechanism of deformation remains essentially unchanged. Deformation was also

observed on other slip systems, both in nanoindentation and in microcompression. However, by 426 °C, deformation had also occurred by the movement of defects running perpendicular to the loading axis. Serrated flow was also observed at all temperatures, but was greatly diminished at 600 °C (Fig. 5), although slip still occurred on the (0 0 1)[0 1 0] slip system, except in one sample where no clear slip plane was apparent.

The yield and the 2% flow stress almost doubled as the temperature increased from 226 to increased by a factor of almost two as the temperature was increased from 226 to 600 °C. This was not thought to be associated with the lateral defects, as they appeared to be initiated at either free surfaces or slip planes, and therefore grew after deformation had started. Instead, it has been suggested that this might arise due to the increasing stability of the o-$Al_{13}Co_4$ with respect to the monoclinic form with increasing temperature, which is consistent with the theoretical predictions that exist.

Acknowledgements

C.W. acknowledges the support of the European Commission under the Marie Curie Intra-European Fellowship HighTempProp. This work was also partly conducted within the European Integrated Centre for the Development of New Metallic Alloys and Compounds (European C-MAC). S.K. gratefully acknowledges the funding of the German Research Council (DFG) through the Cluster of Excellence "Engineering of Advanced Materials" at the University of Erlangen–Nürnberg. Support from the EPSRC/Rolls-Royce Strategic Partnership (EP/H500375/1) is also acknowledged.

References

[1] Heggen M, Deng D, Feuerbacher M. Intermetallics 2007;15:1425.
[2] Roitsch S, Heggen M, Feuerbacher M. Intermetallics 2010;18:1737.
[3] Klein H, Feuerbacher M, Schall P, Urban K. Phys Rev Lett 1999;82:3468.
[4] Heggen M, Houben L, Feuerbacher M. Philos Mag 2008;88:2333.
[5] Heggen M, Houben L, Feuerbacher M. Mat Mater 2010;9:332.
[6] Östlund F, Howie PR, Ghisleni R, Korte S, Leifer K, Clegg WJ, et al. Philos Mag 2011;91:1190.
[7] Östlund F, Rzepiejewska-Malyska K, Leifer K, Hale LM, Tang Y, Ballarini R, et al. Adv Funct Mater 2009;19:2439.
[8] Gille P, Bauer B, Hahne M, Smontara A, Dolinšek J. J Cryst Growth 2011;318:1016.
[9] Wheeler JM, Michler J. Rev Sci Instrum 2013;84:045103.
[10] Wheeler JM, Niederberger C, Tessarek C, Christiansen S, Michler J. Int J Plasticity 2013;40:140.
[11] Wheeler JM, Raghavan R, Michler J. Scr Mater 2012;67:125.
[12] Frost HJ, Ashby MF. Deformation-mechanism maps: the plasticity and creep of metals and ceramics. Oxford: Pergamon Press; 1982.
[13] Korte S, Clegg WJ. Philos Mag 2010;91:1150.
[14] Dimiduk DM, Uchic MD, Parthasarathy TA. Acta Mater 2005;53:4065.
[15] Ragani J, Donnadieu P, Tassin C, Blandin JJ. Scr Mater 2011;65:253.
[16] Bouvier S, Needleman A. Model Simul Mater Sci 2006;14:1105.
[17] Gödecke T, Ellner M. Z Metallkd 1996;87:854.
[18] Caillard D, Martin JL. Thermally activated mechanisms in crystal plasticity. Amsterdam: Elsevier Science; 2003.
[19] Louchet F. Philos Mag A 1995;72:905.
[20] Mihalkovič M, Widom M. Phys Rev B 2007;75:014207.
[21] Fleischer F, Weber T, Jung DY, Steurer W. J Alloys Compd 2010;500:153.